THE JOURNAL OF PHYSICAL CHEMISTRY C

Article

pubs.acs.org/JPCC

Plasmonic Sensing via Photoluminescence of Individual Gold Nanorod

Guowei Lu,* Lei Hou, Tianyue Zhang, Jie Liu, Hongming Shen, Chunxiong Luo, and Qihuang Gong*

State Key Laboratory for Mesoscopic Physics, Department of Physics, Peking University, Beijing 100871, China

Supporting Information

ABSTRACT: Label-free plasmonic sensors based on localized surface plasmon resonances of nanostructured noble metal materials usually transduce optical refractive index changes occurring in the vicinity of the nanostructures by optical scattering or by extinction. We demonstrate in experiments that the photoluminescence of plasmonic nanoparticles can also be employed to detect biological molecule binding events efficiently. Photoluminescence probably due to plasmon emission of a single gold nanorod presents a similar resonance peak and resembles the response to a refractive index change observed by scattering. The well-known biotin−streptavidin binding assay was detected successfully using the photoluminescence of an individual isolated nanorod. The localized surface plasmon resonances' responses by scattering *in situ* with the same nanorod and control experiments were also performed to verify the sensing process. The results evidence that a nanoscale plasmonic sensor can also be archived effectively through the photoluminescence of a single plasmonic nanostructure. Furthermore, key parameters to optimize the photoluminescence based label-free plasmonic sensing are discussed in detail. The photoluminescence provides an alternative way for label-free plasmonic sensing. And it is believed that further exploration of this concept could lead to a whole new class of efficient plasmonic sensors with diverse and novel functionalities.

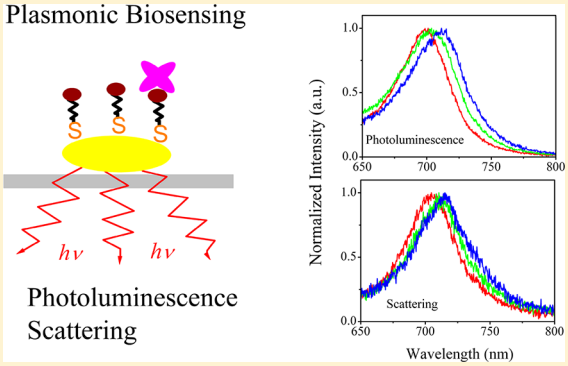

INTRODUCTION

Plasmonic nanostructures support localized surface plasmon resonances (LSPR), which are associated with collective oscillations of free electrons and lead to unique optical properties to route and manipulate light at nanometer length scales.[1,2] The undisputed distinctive optical properties of plasmonic nanostructures have allowed for rapid advances in many interdisciplinary subjects, such as surface enhanced spectroscopy, solar energy conversion, integrated optical nanocircuitry, LSPR sensing, etc. Among them, the photoluminescence (PL) of the plasmonic nanostructure itself is of great interest.[3] Visible PL from bulk metals shows very little quantum efficiency ($\sim 10^{-10}$), probably because the nonradiative energy relaxation processes in metals are much faster than radiative electron hole recombination.[4,5] It is well-known that the physical and chemical properties of small assemblies of atoms often differ from those of the corresponding bulk materials. For instance, the PL efficiencies on the order of 10^{-4} have recently been observed for gold nanorod colloids.[6] And, it has also been reported that nanosized gold clusters show a significant high quantum yield, for example, up to ~41% for Au_8 clusters stabilized in dendrimer aqueous solution, which is not predicted by classical Mie theory but is expected to involve a quantum confinement effect.[7] We focus our attention on the PL of plasmonic nanoparticles with dimension scale of tens of nanometers due to their stability and controllability compared to the nanosized clusters.

Light emission from plasmonic nanostructures can be excited usually by electrons (e.g., in cathodoluminescence spectroscopy[8]) or photons (e.g., in one-photon or two-photon luminescence[9−16]). The visible luminescence could be explained by interband transitions of d-band electrons into the conduction band and subsequent radiative recombination or be assigned to a process in which excited d-band holes recombine nonradiatively with sp electrons and subsequent radiative decay of the surface plasmons, i.e., a plasmon emission process.[14−16] Although the PL mechanism of plasmonic nanoparticles is not yet understood unambiguously, it is believed that the light emission is truly related to the LSPR of the plasmonic nanostructures. For application purposes, the luminescence of the plasmonic antennae (often excited by cathodoluminescence or two-photon luminescence) itself is a useful characteristic that has already been utilized to investigate the plasmon resonance behaviors in the visible near-infrared spectral regime.[8−10] Highly efficient photoluminescence generated from plasmonic nanoparticles has also led to its widespread application in biological labeling and imaging[11,12] or as a probe in fluorescent correlation spectroscopy for the measurement of its rotational and translational dynamics.[16] To date, the label-free plasmonic sensors that transduce molecular binding events at their surface

Received: September 23, 2012
Revised: October 29, 2012
Published: November 7, 2012

ACS Publications © 2012 American Chemical Society

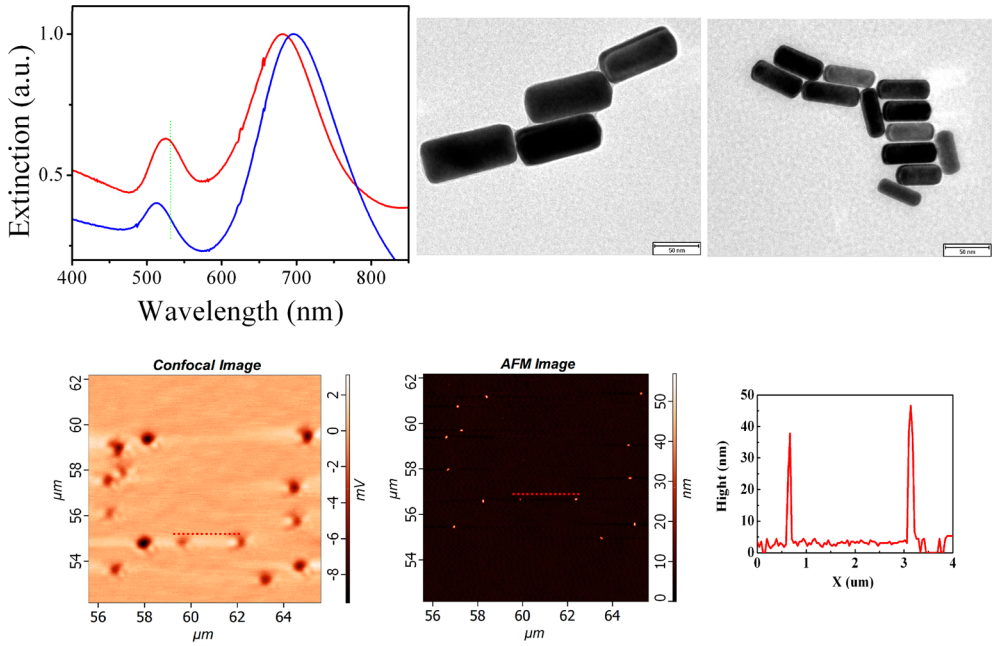

Figure 1. (top) TEM images and extinction spectra of gold nanorods in solution. The average diameter, length, and aspect ratio are 30 ± 2, 70 ± 5, and 2.5 for the large nanorods and 16 ± 3, 50 ± 5, and ~3 nm for the small nanorods, respectively. The scale bar is 50 nm in both TEM images. (bottom) Optical confocal scanning image and corresponding atomic force microscopy image of the large nanorods immobilized on a coverslip with 10 μm × 10 μm scanning area and cross-section line as indicated in the scanning images. The heights of the nanorods are 30–40 nm, which is in good agreement with the TEM measurements.

into macroscopically measurable optical signals mostly based on the light scattering or absorption properties of the metallic nanostructures because their resonance frequencies are functions of the local environment refractive index. This approach to achieve label-free sensing, at the beginning proposed for ensemble colloids, was then demonstrated for immobilized nanoparticles on a transparent substrate and was recently extended to the limit of single plasmonic nanoparticles. For instance, gas adsorption or reactions at a metallic surface are detected through the changing optical properties of the metallic nanosystem on gas exposure.[17,18] A wide variety of molecular surface binding events, including DNA hybridization, carbohydrate–protein binding, and antigen–antibody interactions, have been detected and characterized successfully with plasmonic nanosensors.[19−23] Silver nanoprism arrays fabricated using nanosphere lithography are sufficiently sensitive to detect protein conformational changes.[24] Furthermore, by using an intense white light laser source and intensified CCD camera, Ament et al. have improved the sensitivity limit of the single plasmonic nanoparticle sensor to detect a single large size protein.[25] The label-free plasmonic sensors based on the light scattering or absorption properties of the metallic nanostructures have presented great potential applications in biological detection.

However, the PL characteristic of the plasmonic nanoparticles has never been exploited for the biosensing purposes. In this study, label-free plasmonic sensing of standard biotin–streptavidin recognition is demonstrated in experiments based on the PL spectra of a single plasmonic nanoparticle. The PL of plasmonic nanoparticles was demonstrated to resemble closely the surface plasmon scattering behaviors of the metallic nanostructures. The experimental results convinced that PL of the plasmonic nanoparticles is able to efficiently transduce the molecular binding events (similar to the light scattering or absorption spectra) for plasmonic biosensing. The PL spectra of plasmonic nanoparticles can be served as an alterative way for plasmonic sensing except for the scattering spectra. In fact, the basic concept of plasmonic sensing by the PL spectra is generic and can be applied to a wide range of plasmonic nanostructures. We believe that further exploration of this concept could lead to a whole new class of efficient plasmonic sensors with diverse and novel functionalities.

EXPERIMENTAL METHODS

Sample Preparation. All chemicals were obtained from commercial sources and were used without further purification. Gold nanorods are synthesized by seed-mediated method.[26] Briefly, a gold seed solution was prepared by adding rapidly 0.6 mL of 0.01 M ice-cold $NaBH_4$ solution into a mixture containing 10 mL of 0.1 M CTAB and 0.25 mL of 10 mM $HAuCl_4$ and then was kept still at 25 °C for 2 h. The growth solution was prepared by mixing 2 mL of 10 mM $HAuCl_4$, 40 mL of 0.1 M CTAB, 0.32 mL of 0.1 M VC, and 0.2 mL of 0.01 M $AgNO_3$ together. For gold nanorods' growth, 10 or 20 μL seed solution was added into the growth solution and left undisturbed at 27 °C for 16 h. After growth, gold nanorods were washed and purified by centrifugation at 14 000 rpm and then dispersed in pure water. Glass substrate with isolated gold nanorods on its surface was prepared according to our previous report.[27] At first, the cover glass was washed by supersonic in detergent, acetone, alcohol, and pure water. Then it was immersed in 5 vol % MPTMS alcohol solution for 15 min. Excessive MPTMS was removed by supersonic in alcohol. The interval between individual immobilized rods was found to be a function of the immersing time, concentration of gold nanorods, and incubation time. The surface silanization cover glass was immersed in as prepared gold nanorods' solution for a short time (about 3–5 s) and was washed thoroughly by alcohol or pure water to remove unbonded nanorods.

dx.doi.org/10.1021/jp309450b | J. Phys. Chem. C 2012, 116, 25509–25516

Spectral Measurements of a Single Gold Nanorod. The dark-field scattering and PL spectra techniques were integrated into the same microspectroscopy system based on an inverted optical microscope (NTEGRA Spectra, NT-MDT). As schematically shown in Figure 1a, the scattering spectra of plasmonic nanoparticles were measured using a white light total internal reflection scattering method based on a high numerical aperture oil-immersion objective lens (NA 1.49, 60× TIRF, Olympus, Japan). A collimated white light beam was approximately focused at the objective's back focal plane, and the scattering signal was collected by the same objective lens and directed into a spectrometer with a cooled spectroscopy CCD (iDdus, Andor).[28,29] Meanwhile, the microspectroscopy system is able to switch easily from scattering spectrum measurement to PL spectrum measurement excited by a CW laser at λ = 532 or 633 nm *in situ* for the same nanoparticles. For comparison, the exposure time was 30 s, the same for scattering and PL spectra measurements. Additionally, the microspectroscopy system was also integrated with a scanning probe head, which allowed us to characterize the plasmonic nanoparticle with nanometer resolution. Thus, the microspectroscopy system can be used to investigate the plasmonic sensing ability based on the PL spectra or based on the conventional optical scattering spectra of the same plasmonic nanoparticle. The acquired spectra at 30 s intervals with about 100 nm spectral region around the peak was fitted by Lorentz or a fifth-order polynomial, and then the centroid of the peak was calculated for the maximum wavelength; the temporal resolution was about tens of seconds.[30,31]

Numerical Simulations. The finite-difference time-domain (FDTD) method was used to calculate the LSPR characteristics of individual nanostructures. The optical dielectric function of the gold material was modeled using a Drude–Lorentz dispersion function. The refractive index of the surrounding media is taken to be 1.33 for water in all simulations. The LSPR of gold nanorods are calculated and the structure drawn as a cylinder with two semispherical caps.

RESULTS AND DISCUSSION

To develop plasmonic nanosensors using the PL property, we made efforts to investigate a single isolated immobilized nanoparticle because the LSPR width of a single nanoparticle is narrow with respective to large ensembles of colloid nanoparticles which benefits the sensing ability.[25,32−34] Given that the system uncertainty is established, the overall performance of the single plasmonic nanoparticle sensor is dependent on the parameters of the nanoparticles used in the experiments.[30] In our experiments, rod-shaped gold nanoparticles were utilized because of the tunable and narrow longitudinal plasmon resonance band in the visible and near-infrared spectral regions. Recent studies have reported that gold nanorods present high efficiency of the light emission, and the response of the PL spectral to the refraction index changes which is similar to that observed by optical scattering.[11−16] Here, the gold nanorods were chemically synthesized by a seed-mediated growth procedure.[26] The synthesized materials were characterized by TEM and extinction spectra as shown in Figure 1. Two kinds of nanorods were obtained with different size: i.e., large size nanorods with diameter of ∼30 nm and length of ∼70 nm, whose longitudinal LSPR peak is ∼682 nm in colloid solution, and small size nanorods with diameter of ∼16 nm and length of ∼50 nm, whose longitudinal surface plasmon resonance peak is ∼698 nm.

A microspectroscopy system (NTEGRA Spectra, NT-MDT) based on an inverted optical microscope was developed to integrate the dark-field scattering, PL spectra, confocal scanning, and atomic force microscopy (AFM) techniques together, as schematically shown in Scheme 1a, which allows us

Scheme 1. (a) Diagram of the Microspectroscopy System Used in the Present Study, Equipped with Multiple Measurement Capabilities Including White Light Total Internal Reflection Scattering, Photoluminescence, Optical Confocal Scanning Imaging, and Scanning Probe Spectroscopy Imaging; (b) Schematic Representation of the Biosensing Process of a Specific Biotin−Streptavidin Affinity Model with a Single Immobilized Nanorod

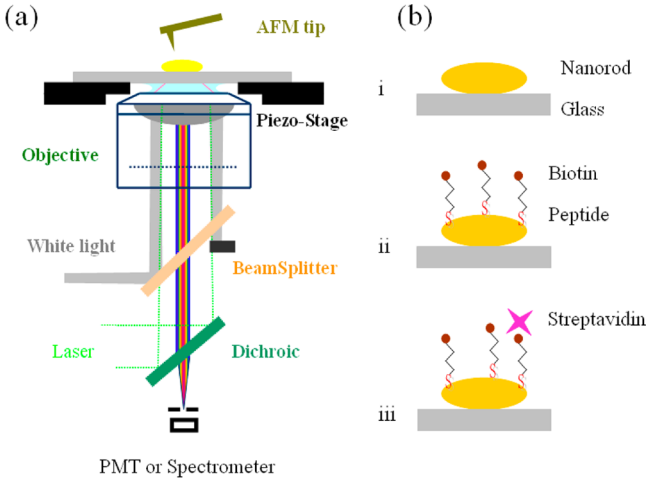

identify a single isolated nanoparticle and measure *in situ* the scattering and PL spectra of the same individual nanoparticle.[28,29] The synthesized nanorods were immobilized onto glass coverslips in a manner similar to our previous report for gold nanoparticles with an average interparticle spacing of several micrometers.[27] Such an interparticle spacing is suitable for interrogation of isolated nanorods by the microspectroscopy system because the diffraction-limited spots are sufficiently separated so as not to overlap. First, the gold nanorod-immobilized coverslips were characterized simultaneously using the optical confocal scanning image and AFM technique as performed in the tip-enhanced Raman scattering measurements, and typical results are shown in Figure 1, bottom. As can be seen, most of the nanorods are isolated and well immobilized onto the glass surface, as previously reported for gold nanoparticles,[27] and the height of the nanorods obtained by AFM is in good agreement with the TEM results. Hence, the isolated nanorods can be located and distinguished actually by the confocal scanning image solely, which is convenient during the biosensing measurements. Then optical scattering and PL spectra of the same individual isolated nanoparticle can be obtained for further biosensing experiments.

The confocal scanning imaging method utilized here to locate the nanoparticle is mainly based on the interference between the background reflection by the interface and the scattered field by the nanoparticles.[35] Such interferometric detection scheme is wavelength dependence of the plasmon resonances of the nanoparticles. The confocal scanning image in Figure 1 is obtained for the large nanorods, while the image contrast for the small nanorods is not obvious as the former.

dx.doi.org/10.1021/jp309450b | J. Phys. Chem. C 2012, 116, 25509−25516

Because the transverse resonances of the small nanorods present low intensity and overlap less with the illumination laser of wavelength at 532 nm. The confocal scanning image method can be improved by subtracting the signals of the laser intensity fluctuations to reduce root-mean-square for the small nanoparticle detection.[36] Hence, the large nanorods with diameter of ~30 nm were chosen to be utilized mainly in this study for biosensing experiments; this size is an optimized dimension scale for scattering type plasmonic sensors.[28,30] Moreover, in order to verify the biosensing ability via the PL of a single gold nanorod, the biosensing process based on the conventional scattering spectrum was also performed *in situ* with the same nanoparticle.

First, the PL properties of single isolated nanorods were studied in detail. During regular surface enhanced Raman scattering measurements, there is often a strong broad background which should be ascribed partially to the light emission of the metallic nanostructures. As can be seen from Figure S1, the PL spectrum obtained for a single isolated nanorod shows a clear resonance peak, which interestingly resembles the scattering spectrum that is obtained for the same nanorod after the background spectrum taken in the absence of the nanorod is subtracted. The observed PL spectrum is believed to be due to the plasmon emission of the gold nanorods because the resemblance is maintained, irrespective of the excitation laser wavelength (532 or 633 nm) or the refractive index of the medium used, as discussed in a previous study.[16] Furthermore, the excitation power and polarization dependent on the PL spectra were also carried out (see Figure S2) and found to be consistent with previous reports.[16] The PL peak shape of the nanorods in aqueous medium is stable when the excitation power is less than about 1 mW (the threshold of thermal reshaping varies for different nanorods).[13] The PL spectrum of the immobilized nanorod does not show any signs of intensity blinking, which inherits the intrinsic stability property of plasmon resonance scattering or absorption spectrum.

To explore the possibility of plasmonic sensing based on the PL of the nanorods, the environmental refractive index around the immobilized nanorods were changed first. Typical white light scattering and PL spectra of the same nanorod are shown in Figure 2, which were measured in air (refractive index n = 1.0), water (n = 1.33), and glycerol (n = 1.47). The PL spectrum red-shifts with change of dielectric constant of the surrounding medium in the same way as observed in the corresponding scattering spectrum. The results mean that like the scattering or absorption spectrum, the PL spectrum of the nanorod also responses effectively to the changes of the environmental refractive index. It is well-known that the bulk refractive index sensitivity of a plasmonic sensor in response to the changes in the refractive index can be described approximately according to the equation

$$\lambda_{LSPR} = \lambda_0 + m\Delta n \quad (1)$$

where λ_{LSPR} is the plasmon resonance maximum of the nanostructure, m is the sensitivity factor, and Δn represents the change in refractive index. The sensitivity factor m of the nanorod shown in Figure 2 inset is obtained at about 210 nm/RIU (RIU = refractive index unit) even though the influence of the glass substrate is not taken into account. Actually, the bulk refractive index sensitivity is affected by the glass substrate, whereas the local sensing ability of the nanorod is not affected by the substrate because of the additivity property of plasmonic sensing.[37] The results mean that the PL spectrum of the gold nanorod could be a new way to realize label-free plasmonic sensing.

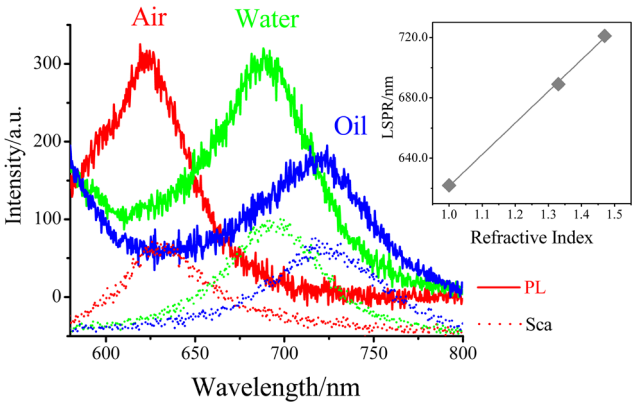

Figure 2. Photoluminescence (solid lines) and scattering (dots) spectra of the same isolated individual gold nanorod immersed in different medium, i.e., air (red), water (green), and glycerol (blue). The inset show the LSPR peak of the nanorod in different medium and the fitting line using eq 1.

To demonstrate the capability of biosensing based on the PL of a single gold nanorod, we investigated the standard biological binding event of streptavidin to a biotin-functionalized gold nanorod as shown schematically in Scheme 1b. Thiolated peptides (five amino acid chain from Chinese-Peptide Co., China) modified with a biotin molecule at their respective N-terminal ends were immobilized onto the gold nanorod surface through the thiol groups of the cysteine residues.[38] Then, streptavidin as a detection target (Sigma-Aldrich, China) at different concentrations was introduced into a polydimethylsiloxane (PDMS) microfluidic channel containing the biotinylated gold nanorods. Figure 3a shows three representative spectra obtained from a streptavidin detection measurements with the PL of the gold nanorod. The first spectrum was obtained in the PBS solution before modifying the nanorods with the thiolated peptide biotin. The second spectrum was obtained after the biotin was conjugated to the nanorods, and the shift of the PL peak was attributed to the successful conjugation of the biotin group to the gold nanorod. The third spectrum was obtained after the nanorod was incubated in a PBS solution with 100 nM streptavidin. The streptavidin binding to the surface of the biotinylated nanorod resulted in a ~6.0 nm red-shift of the nanorod PL peak. For comparison and verification, regular plasmonic sensing based on scattering was also performed *in situ* for the same nanorod and the process. The results are shown in Figure 3b. The biosensing results obtained by scattering are in good agreement with the results obtained using the PL spectral method. To this end, we demonstrate that the plasmonic sensing based on the PL spectrum of a single gold nanorod is feasible and is as efficient as that performed by scattering.

Moreover, the PL peak red-shifts for 50 and 10 nM streptavidin are ~4.0 and ~1.0 nm, respectively, as shown in Figure 3c. The results obtained by PL and scattering are in agreement with previous study.[32] And, as can be seen from the time-resolved spectral acquisition shown in Figure 3d, the streptavidin binding process was completed mainly within several secondes. It should be noted that there is a slow slight increase of the LSPR peak as the incubation time increases due

dx.doi.org/10.1021/jp309450b | J. Phys. Chem. C 2012, 116, 25509–25516

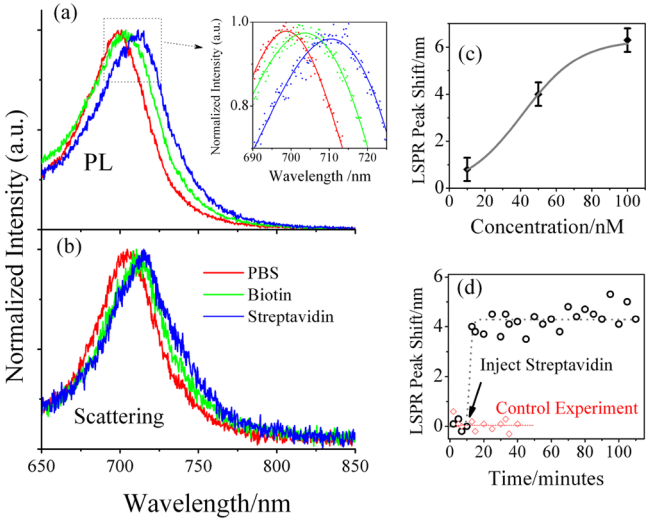

Figure 3. Plasmonic biosensing based on the PL and scattering spectra of a single gold nanorod. (a) PL spectra of a single gold nanorod after sequential incubation in PBS solution (red), thiolated peptide with a biotin label (green), and 100 nM streptavidin (blue). The inset shows the enlarged normalized spectra and the fitting curves of the peak centroid of the PL spectra. (b) Scattering spectra of the same nanoparticle measured correspondingly after each PL spectra for comparison. (c) The PL spectra red-shift as the concentration of streptavidin solution increases. (d) Time measurement of the PL spectral peak centroid shift of a single biotin-conjugated gold nanorod incubated in 50 nM streptavidin in PBS solution; time measurement of the control experiments using biotin-saturated streptavidin is also presented for comparison.

to the saturation of streptavidin bonding process. The result of time-resolved LSPR measurement is in agreement with a previous report,[32] whereas time resolution of our optical setup (>30 s) is unable to capture discrete single molecule binding events because of the fast association processes of biotin−streptavidin assay. Fortunately, by using a cross-correlation function approach, single molecule LSPR detection was demonstrated by monitoring antibody−antigen unbinding process through the scattering spectra of individual gold bipyramid.[39] In principle, this approach should also be applicable to the plasmonic sensing by the PL signal. In addition, control experiments using biotin-saturated streptavidin were also performed to verify the PL detection scheme. The characteristic scattering and PL spectral peak red-shift resulting from the biotin adsorption were observed clearly as described above, but there was no further red-shift in the PL spectral peak upon incubation with the biotin-saturated streptavidin as shown in Figure S4, nor was there an observed peak shift during the streptavidin incubation process for non-biotin-functionalized nanorods. These results provide strong evidence to suggest that the PL spectral peak red-shifts of a single nanorod observed in the streptavidin binding to the biotin-functionalized nanorods are caused by the specific biomolecular recognition between biotin and streptavidin.

It should be noted that the detection limit of our system (defined here as the lowest concentration of analyte) is unable to detect lower concentrations of streptavidin to the sub-nanomolar level as previous reports.[30] The main reason is due to the drift of the microscope focus and the sample stage, which lead to a large uncertainty, especially, a tightly focused laser spot was used in the PL measurements.[31] The algorithmic fitting uncertainty of the PL spectral peak can as low as ∼0.01 nm, whereas the noise level for the PL signal is about 0.3 nm as shown in Figure S3a (simply obtained by the maximum and minimum value of the measured data series) when the PL spectra of the same nanoparticle were acquired continuously without moving the sample stage. But the noise level was deteriorated as shown in Figure S3c when the PL spectra of the same nanoparticle were acquired after moving the stage back and forth (the moving of the sample was necessary sometimes when a lot of nanoparticles were needed to be measured and compared on a chip), which is due to the sample stage restoration and the fluctuation of laser power. Hence, the total uncertainty of our detection system increases to ∼0.8 nm if we move back and forth between several different nanoparticles, typical result of one particle as shown in Figure S3 and Figure 3d. On the contrary, the noise level is almost the same for the scattering spectra whether the stage is moved or not as shown Figure S3b,d. Probably, the illumination area of total inter-reflection white light is large enough to suppress the stage drift effect. So that the noise level of the PL spectra is comparable to the scattering, which can be improved by using defocused laser spot and stable laser source and by improving the physical stability of the system. Nevertheless, we think that the PL emission of a single plasmonic nanoparticle is a promising alternative way for sensitive biosensing except for the scattering spectrum.

Additionally, the oil-immersion objective lens was replaced with a water immersion objective lens (NA 1.2, 60×, PlanApo, Olympus) to collect the nanorod's PL spectrum in different refractive index medium. The results indicate that the PL intensity acquired by the water immersion objective is comparable to that by the oil objective, and the PL spectra in different medium can still be performed well as shown Figure 4a, whereas the PL intensity of the nanorods reduces obviously when an air objective (NA 0.8) was utilized. (The data are not shown here for comparison because the PL spectra by different objective were not from the same nanoparticles.) The PL emission exhibits a perfect dipole behavior near the substrate surface. The conversion of evanescent into propagating field components near an interface leads to the angular distribution of emission concentrated mostly around at the critical angle. Hence, the collected signal intensity decreases as the refractive index of medium increasing because of the increase of the critical angle as shown in Figure 4. To further understand the emission behavior, individual gold nanorod is assumed as a dipole; we simulate the Fourier image of a dipole emission using analytical expressions.[40] The results shown in the bottom of Figure 4 present the far-field angular distribution of a dipole near air/glass and water/glass interface. Therefore, to apply the PL of a single nanoparticle, it is very helpful to use high NA objectives for a high signal noise ratio; this result is consistent with the report about surface-enhanced Raman scattering from individual nanoparticle.[41] The results mean that plasmonic sensing by a single plasmonic nanostructure can also be achieved independently using a conventional confocal fluorescence microscope platform, which would be convenient for chemical or biological detection analysis. For example, plasmonic nanoparticles could be used as bright imaging labels on account of their high PL emission and simultaneously used as a plasmonic nanosensor for intracellular detection, especially those plasmonic nanoparticles that can be manipulated under optical trapping control.[42]

The PL spectra of the small nanorods were also measured for comparison even though the contrast of the confocal scanning

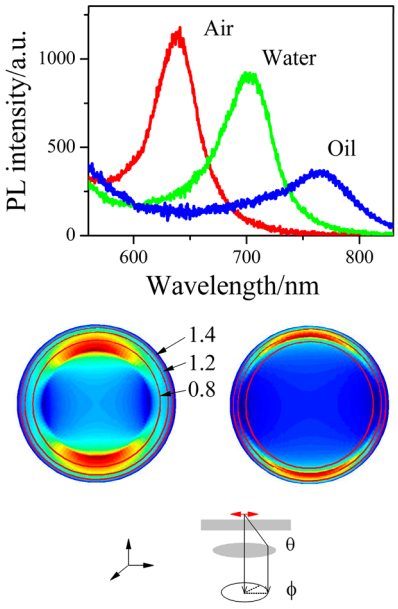

Figure 4. (top) PL spectra of the same individual nanorod in different surrounding media with water-immersed objective (NA 1.2, 60×). (bottom) Fourier image of the dipole oriented horizontally, radiating at λ = 650 nm and located at a distance 10 nm from the air/glass interface (left) and water/glass interface (right), respectively. The red lines indicate the corresponding collection angles of NA = 0.8, 1.2, and 1.45. The scheme of the angle-resolved PL emission detection is also presented.

image was lower than the large nanorods. It was found that the PL intensity is still high for the small size nanorods, as shown Figure 5a, while the scattering intensity decrease greatly. This is probably due to the difference in the relation between the scattering and absorption cross section as a function of

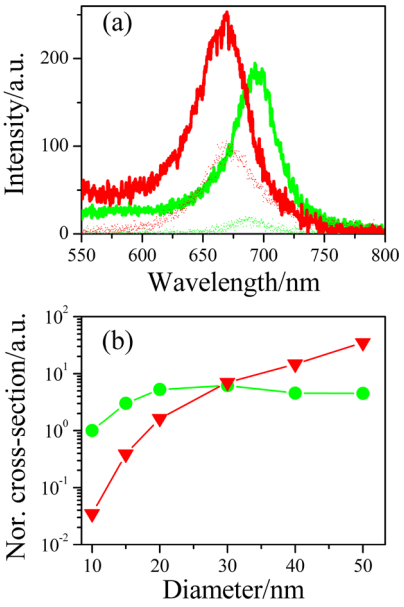

Figure 5. (a) Typical PL (solid lines) and scattering (dots) spectra of a single nanorod for large nanorod (red) and for small nanorod (green). (b) The scattering (red) and absorption (green) coefficients of various size nanorods. All coefficients are normalized by the absorption coefficient of the nanorod with diameter of 10 nm and length of 30 nm.

nanoparticle size.[43] To better understand this size effect, the absorption and scattering cross section of gold nanorods with different size are calculated employing finite-difference time-domain (FDTD) method.[35,44] The nanorods have various diameters but with the same aspect ratio of 3; the longitudinal dipolar LSPR are presented in Figure S5. The normalized absorption and scattering cross-section coefficients are shown in Figure 5b. As the dimension size decreasing from 30 to 15 nm, the scattering cross section decreases significantly as compared to the absorption cross section. This result implies that small sized plasmonic nanoparticle for the PL spectrum is also applicable as an effective plasmonic sensor. This is helpful for sensing performance because of the smaller sensing volume of small sized nanorod, which usually results in a high local sensitivity.[30,35] On the contrary, the plasmonic sensor based on scattering signal has to often use a relative large size nanoparticle to obtain enough scattering signal intensity. The PL intensity can be described approximately as $S_{PL} = \kappa I_{ex}\sigma_{abs-ex}Q$, where I_{ex} is the excitation laser power intensity, σ_{abs-ex} is the absorption cross section of the nanoparticle at the excitation wavelength, and Q is the quantum yield efficiency of the nanoparticle. For a single gold nanorod, although the quantum yield efficiency Q of the nanorod (at the order of 10^{-4}) is very low with respect to the dye molecule, the absorption cross-section σ_{abs-ex} of the nanoparticle (at the order of 10^{-11} cm^2) is significantly larger than the dye molecule (at the order of 10^{-16} cm^2). Thus, a single nanorod is often brighter than a single dye molecule,[43] and the high light emission provides an adequate signal-to-noise ratio for biosensing application as demonstrated in this study. It should be noted that the plasmonic sensitivity based on the PL in this study cannot be comparable with that by the optimized scattering experiment by Ament et al., where with the help of an intense light source, an intensified CCD camera and larger size nanorod, etc., they have pushed the sensitivity limit of the single plasmonic nanoparticle sensor to a single biological molecule level detection.[25]

As an alternative way to achieve label-free plasmonic sensor, we think that the sensitivity of plasmonic biosensing based on the PL spectra can be improved further rather than current results. First, a higher σ_{abs-ex} is better to improve the PL signal intensity: (i) By adjusting the wavelength of the excitation laser source, the PL intensity excited by the laser at λ = 633 nm is obviously higher than that excited by the laser at λ = 532 nm with the same input laser power, as shown in Figure S2. (ii) Using other plasmonic nanostructures such as rattles, nanocubes, silver particles, or plasmonic hot spots, a larger absorption cross section σ_{abs-ex} and a higher light emission efficiency Q are expected to further improve the PL performances.[45−49] Second, with the help of optical antenna design in theory, the PL emission pattern of the plasmonic nanostructure in far field can be beamed which would lead to bright unidirectional signal, resulting in an increased collection efficiency κ. Third, the multiphoton PL process, especially two-photon luminescence method where the fluorescence signal is squared dependent on the excitation power intensity and nonspecific background is low, could also be effective for plasmon emission sensing in principle, which represents a promising way to improve the sensor sensitivity. Finally, with the help of specific surface treatment, the analytes can be precisely grafted onto the highest sensitive area because of plasmonic nanoparticles' anisotropic plasmonic sensing property,[30,35] which has been applied successfully for single

molecule detection by surface-enhanced Raman scattering and a sensitive photothermal assay.[50,51] These efforts are currently being conducted to optimize the plasmonic sensing capability based on the PL spectra.

CONCLUSIONS

In summary, we demonstrated that the PL spectrum due to plasmon emission of a single gold nanorod presents a similar resonance peak and resembles the response to refractive index change as that by the white light scattering spectrum. This intrinsic property can be utilized to transduce biological molecular binding events, and the results show that the biosensing application is feasible and efficient. Although our present system with high noise level is not able to distinguish lower concentration analytes as can be achieved in previous studies, it is believed that the performance of plasmonic biosensing by the PL spectrum is comparable to that afforded by scattering. And label-free plasmonic sensing based on the PL spectrum can be optimized further through a series of key parameters. These results mark the first time in principle that plasmonic biosensing can be realized with the photoluminescence of a single plasmonic nanoparticle and open a new way to achieve convenient and sensitive label-free plasmonic sensors.

ASSOCIATED CONTENT

Supporting Information

Corrections of the photoluminescence and scattering spectra; the excitation power and polarization dependent on the nanorods' photoluminescence excited by laser at wavelength of 532 and 633 nm, respectively; the control experiment results by incubating in biotin-saturated streptavidin; the detection limit and noise level of the optical system; the absorption and scattering spectra of the nanorods calculated by the FDTD method. This material is available free of charge via the Internet at http://pubs.acs.org.

AUTHOR INFORMATION

Corresponding Author

*E-mail: guowei.lu@pku.edu.cn (G.L.); qhgong@pku.edu.cn (Q.G.).

Notes

The authors declare no competing financial interest.

ACKNOWLEDGMENTS

This work was supported by the National Key Basic Research Program of China (grants 2013CB328703 and 2009CB930504) and the National Natural Science Foundation of China (grants 61008026, 11121091, and 90921008).

REFERENCES

(1) Anker, J. N.; Hall, W. P.; Lyandres, O.; Shah, N. C.; Zhao, J.; Van Duyne, R. P. *Nat. Mater.* **2008**, *7*, 442−453.
(2) Schuller, J. A.; Barnard, E. S.; Cai, W.; Jun, Y. C.; White, J. S.; Brongersma, M. L. *Nat. Mater.* **2010**, *9*, 193−204.
(3) Gaiduk, A.; Ruijgrok, V. P.; Yorulmaz, M.; Orrit, M. *Phys. Chem. Chem. Phys.* **2011**, *13*, 149−153.
(4) Mooradian, A. *Phys. Rev. Lett.* **1969**, *22*, 185−187.
(5) Boyd, G. T.; Yu, Z. H.; Shen, Y. R. *Phys. Rev. B* **1986**, *33*, 7923−7936.
(6) Mohamed, M. B.; Volkov, V.; Link, S.; El-Sayed, M. A. *Chem. Phys. Lett.* **2000**, *317*, 517−523.
(7) Wilcoxon, J. P.; Martin, J. E.; Parsapour, F.; Wiedenman, B.; Kelley, D. F. *J. Chem. Phys.* **1998**, *108*, 9137−9143.
(8) Yamamoto, N.; Araya, K.; Garcia de Abajo, F. J. *Phys. Rev. B* **2001**, *64*, 205419.
(9) Muhlschlegel, P.; Eisler, H.-J.; Martin, O.; Hecht, B.; Pohl, D. *Science* **2005**, *308*, 1607−1609.
(10) Imura, K.; Okamoto, H. *J. Phys. Chem. C* **2009**, *113*, 11756−11759.
(11) Wissert, M. D.; Ilin, K. S.; Siegel, M.; Lemmer, U.; Eisler, H. J. *Nano Lett.* **2010**, *10*, 4161−4165.
(12) Wang, H. F.; Huff, T. B.; Zweifel, D. A.; He, W.; Low, P. S.; Wei, A.; Cheng, J. X. *Proc. Natl. Acad. Sci. U. S. A.* **2005**, *102*, 15752−15756.
(13) Bouhelier, A.; Bachelot, R.; Lerondel, G.; Kostcheev, S.; Royer, P.; Wiederrecht, G. P. *Phys. Rev. Lett.* **2005**, *95*, 267405.
(14) Beversluis, M. R.; Bouhelier, A.; Novotny, L. *Phys. Rev. B* **2003**, *68*, 115433.
(15) Dulkeith, E.; Niedereichholz, T.; Klar, T. A.; Feldmann, J.; von Plessen, G.; Gittins, D. I.; Mayya, K. S.; Caruso, F. *Phys. Rev. B* **2004**, *70*, 205424.
(16) Tcherniak, A.; Dominguez-Medina, S.; Chang, W.-S.; Swanglap, P.; Slaughter, L. S.; Landes, C. F.; Link, S. *J. Phys. Chem. C* **2011**, *115*, 15938−15949.
(17) Larsson, E. M.; Langhammer, C.; Zoric, I.; Kasemo, B. *Science* **2009**, *326*, 1091−1094.
(18) Liu, N.; Tang, M. L.; Hentschel, M.; Giessen, H.; Alivisatos, A. P. *Nat. Mater.* **2011**, *10*, 631−636.
(19) Elghanian, R.; Storhoff, J. J.; Mucic, R. C.; Letsinger, R. L.; Mirkin, C. A. *Science* **1997**, *277*, 1078−1081.
(20) Sannomiya, T.; Voros, J. *Trends Biotechnol.* **2011**, *29*, 343−351.
(21) Kalyuzhny, G.; Schneeweiss, M. A.; Shanzer, A.; Vaskevich, A.; Rubinstein, I. *J. Am. Chem. Soc.* **2001**, *123*, 3177−3178.
(22) Lu, G.; Cheng, B.; Shen, H.; Zhou, Y.; Chen, Z.; Yang, G.; Tillement, O.; Roux, S.; Perriat, P. *Appl. Phys. Lett.* **2006**, *88*, 023903−023905.
(23) Okamoto, T.; Yamaguchi, I.; Kobayashi, T. *Opt. Lett.* **2000**, *25*, 372−374.
(24) Hall, W. P.; Anker, J. N.; Lin, Y.; Modica, J.; Mrksich, M.; Van Duyne, R. P. *J. Am. Chem. Soc.* **2008**, *130*, 5836−5837.
(25) Ament, I.; Prasad, J.; Henkel, A.; Schmachtel, S.; Sonnichsen, C. *Nano Lett.* **2012**, *12*, 1092−1095.
(26) Busbee, B. D.; Obare, S. O.; Murphy, C. J. *Adv. Mater.* **2003**, *15*, 414−416.
(27) Wang, Q.; Lu, G.; Hou, L.; Zhang, T.; Luo, C.; Yang, H.; Barbillon, G.; Lei, H. F.; et al. *Chem. Phys. Lett.* **2011**, *503*, 256−261.
(28) Kalkbrenner, T.; Hakanson, U.; Sandoghdar, V. *Nano Lett.* **2004**, *4*, 2309−2314.
(29) Raschke, G.; Kowarik, S.; Franzl, T.; Sonnichsen, C.; Klar, T. A.; Feldmann, J.; Nichtl, A.; Ku1rzinger, K. *Nano Lett.* **2003**, *3*, 935−938.
(30) Nusz, G. J.; Curry, A. C.; Marinakos, S. M.; Wax, A.; Chilkoti, A. *ACS Nano* **2009**, *3*, 795−806.
(31) Dahlin, A. B.; Tegenfeldt, J. O.; Hook, F. *Anal. Chem.* **2006**, *78*, 4416−4423.
(32) Nusz, G. J.; Marinakos, S. M.; Curry, A. C.; Dahlin, A.; Hook, F.; Wax, A.; Chilkoti, A. *Anal. Chem.* **2008**, *80*, 984−989.
(33) Baciu, C. L.; Becker, J.; Janshoff, A.; Sonnichsen, C. *Nano Lett.* **2008**, *8*, 1724−1728.
(34) Sannomiya, T.; Hafner, C.; Voros, J. *Nano Lett.* **2008**, *8*, 3450−3455.
(35) Jacobsen, V.; Stoller, P.; Brunner, C.; Vogel, V.; Sandoghdar, V. *Opt. Express* **2006**, *14*, 405−414.
(36) Kukura, P.; Celebrano, M.; Renn, A.; Sandoghdar, V. *Nano Lett.* **2009**, *9*, 926−929.
(37) Lu, G.; Hou, L.; Zhang, T.; Li, W.; Liu, J.; Perriat, P.; Gong, Q. *J. Phys. Chem. C* **2011**, *115*, 22877−22885.
(38) Lu, G.; Cheng, B.; Shen, H.; Chen, Z.; Yang, G.; Marquette, C. A.; Blum, L. J.; Tillement, O.; Roux, S.; et al. *Appl. Phys. Lett.* **2006**, *89*, 223904−223906.

(39) Mayer, M. K.; Hao, F.; Lee, S.; Nordlander, P.; Hafner, H. J. *Nanotechnology* **2010**, *21*, 255503.
(40) Lieb, M. A.; Zavislan, J. M.; Novotny, L. *J. Opt. Soc. Am. B* **2004**, *21*, 1210−1215.
(41) Shegai, T.; Brian, B.; Miljkovic, V. D.; Kall, M. *ACS Nano* **2011**, *5*, 2036−2042.
(42) Sugiura, T.; Okada, T.; Inouye, Y.; Nakamura, O.; Kawata, S. *Opt. Lett.* **1997**, *22*, 1663−1665.
(43) Boyer, D.; Tamarat, P.; Maali, A.; Lounis, B.; Orrit, M. *Science* **2002**, *297*, 1160−1163.
(44) Taflove, A.; Hagness, S. C. *Computational Electrodynamics: The Finite-Difference Time-Domain Method*, 3rd ed.; Artech House: Norwood, MA, 2005.
(45) Wiley, B.; Sun, Y.; Xia, Y. *Acc. Chem. Res.* **2007**, *40*, 1067−1076.
(46) Wu, X.; Ming, T.; Wang, X.; Wang, P.; Wang, J.; Chen, J. *ACS Nano* **2010**, *4*, 113−120.
(47) Jakab, A.; Rosman, C.; Khalavka, Y.; Becker, J.; Trugler, A.; Hohenester, U.; Sonnichsen, C. *ACS Nano* **2011**, *5*, 6880−6885.
(48) Acimovic, S. S.; Kreuzer, M. P.; Gonzalez, M. U.; Quidant, R. *ACS Nano* **2009**, *3*, 1231−1237.
(49) Chen, C.-D.; Cheng, S.-F; Chau, L.-K.; Wang, C. C. *Biosens. Bioelectron.* **2007**, *22*, 926−932.
(50) Le Ru, C. E.; Grand, J.; Sow, I.; Somerville, R. C. W.; Etchegoin, G. P.; Treguer-Delapierre, M.; Charron, G.; Felidj, N.; Levi, G.; Aubard, J. *Nano Lett.* **2011**, *11*, 5013−5019.
(51) Zijlstra, P.; Paulo, M. R. P.; Orrit, M. *Nat. Nanotechnol.* **2012**, *7*, 379−382.